mathematics

MDPI

Article

Blockwise Joint Detection of Physical Cell Identity and Carrier Frequency Offset for Narrowband IoT Applications

Young-Hwan You [1,*], Yong-An Jung [2], Sung-Hun Lee [2] and Intae Hwang [3,*]

[1] Department of Computer Engineering and Convergence Engineering for Intelligent Drone, Sejong University, Seoul 05006, Republic of Korea
[2] ICT Convergence Research Division, Intelligent Device Research Center, Gumi Electronics & Information Technology Research Institute (GERI), Gumi 39171, Republic of Korea; yajung@geri.re.kr (Y.-A.J.); leesh@geri.re.kr (S.-H.L.)
[3] Department of Electronic Engineering and Department of ICT Convergence System Engineering, College of Engineering, Chonnam National University, Yongbong-ro, Buk-gu, Gwangju 61186, Republic of Korea
* Correspondence: yhyou@sejong.ac.kr (Y.-H.Y.); hit@chonnam.ac.kr (I.H.)

Abstract: This paper presents a novel formulation for detecting the secondary synchronization signal in a narrowband Internet of Things communication system. The proposed approach is supported by a noncoherent algorithm that eliminates the need for channel information. A robust joint synchronization scheme is developed by decoupling the estimations of the physical cell identity and the carrier frequency offset. We derive the detection probability of the proposed physical cell identity detector and the mean squared error of the carrier frequency offset estimator, demonstrating their accuracy through simulation results. The performance of the proposed detection scheme is compared with that of existing detection schemes in terms of both estimation accuracy and computational complexity. Experimental results confirm that the proposed synchronization method exhibits superior performance while maintaining relatively lower complexity compared with benchmark methods.

Keywords: narrowband Internet of Things; secondary synchronization signal; physical cell identity; carrier frequency offset

MSC: 94A13

Citation: You, Y.-H.; Jung, Y.-A.; Lee, S.-H.; Hwang, I. Blockwise Joint Detection of Physical Cell Identity and Carrier Frequency Offset for Narrowband IoT Applications. *Mathematics* **2023**, *11*, 3812. https://doi.org/10.3390/math11183812

Academic Editors: Bin Jiang, Yongxin Liu, Jian Wang and Shuteng Niu

Received: 1 August 2023
Revised: 31 August 2023
Accepted: 2 September 2023
Published: 5 September 2023

1. Introduction

To meet the demands of ultra-low-end Internet of Things (IoT) applications, various low-power wide-area (LPWA) techniques have been developed to operate in licensed frequency bands [1–5]. Among these LPWA standards, narrowband IoT (NB-IoT) stands out as the most promising technique, primarily because of its capability for massive connections inherited from long-term evolution (LTE) [6]. The key features of NB-IoT devices encompass low cost, extensive coverage, narrowband operation, and handling small data volumes [7,8]. Similar to LTE, each device must synchronize with an enhanced base station (eNodeB) to establish a connection to the network. Upon powering up, a user equipment (UE) undergoes a series of procedures to acquire timing information and determine the physical cell identity (PCID) [9–12]. This procedure, encompassing time and frequency estimation in addition to PCID identification, is commonly referred to as the initial cell search in NB-IoT. For this task, a serving eNodeB broadcasts two specialized signals: a narrowband primary synchronization signal (NPSS) and a narrowband secondary synchronization signal (NSSS), both of which the UE must decode.

1.1. Motivations

Before connecting a communication link with the best-serving eNodeB, it is essential for the NB-IoT UE to conduct initial symbol timing offset (STO) and carrier frequency offset

(CFO) detection in the time domain [10–14]. Upon successful completion of this task using the NPSS, the UE proceeds to identify the PCID and gather additional information about the frame structure by performing a search for multiple NSSS sequences. In the event that the UE is unable to identify the NSSS, it has to initiate a complete frequency scan, leading to a significant rise in power consumption [11]. Furthermore, the use of less expensive crystal oscillators in the UE can result in significant time and frequency misalignments between the UE and the eNodeB [12]. Furthermore, when an NB-IoT UE is deployed in either an in-band or guard-band configuration, there is an extra raster offset to consider, which ultimately contributes to an increased CFO [13]. The presence of these ambiguities adds complexity to the process of accomplishing the initial cell search in NB-IoT. Nevertheless, despite encountering substantial ambiguities, an NB-IoT UE is obligated to execute a precise cell search even under conditions of a very low signal-to-noise ratio (SNR). To tackle such a challenge, numerous NSSS synchronization schemes have been extensively investigated in the literature [14–18].

1.2. State of the Art

The NSSS detection strategy can be categorized into two main types: noncoherent detection and coherent detection. Noncoherent detection schemes have been developed assuming a flat-fading condition, as discussed in previous studies [12–18]. The full-search-based approach presented in [12] offers optimal performance; however, it becomes computationally prohibitive due to the exhaustive comparison of all possible combinations of Zadoff–Chu (ZC) and Hadamard–Walsh sequences with the received NSSS sequence. During the initial cell search process, the UE faces the challenge of comparing a large number of potential templates of NSSS to identify the PCID [12]. As a result, the identification of NSSS requires significant computational complexity. To solve a high complexity problem, computationally efficient detection methods have been proposed in [14–17]. These alternatives take advantage of the fact that certain segments of NSSS can be realized without the need for any multiplication operation. The detection schemes proposed in [15–17] leverage the inherent features of the NSSS sequence, leading to a substantial reduction in computational burden compared with the work in [12]. Nevertheless, a significant limitation of these noncoherent estimation approaches is their reduced ability to effectively cope with the frequency selectivity of the channel. In [16], a complexity-effective NSSS detection method using fast Fourier transform (FFT) was proposed for scenarios involving both unknown and estimated channels. Under the assumption of a flat-fading channel, this approach utilizing FFT property can be designed with complexity similar to the noncoherent approach studied in [15]. However, to reduce the effects of frequency-selective fading, employing coherent detection methods imposes a significant computational load during the channel estimation process. In [18], a coherent NSSS detection method was proposed, efficiently decoupling the joint search space of the NSSS detection into a reduced number of hypotheses. This approach significantly reduces arithmetic operations while providing detection ability nearly comparable with the work presented in [16]. More importantly, the two synchronization signals (SSs), NPSS and NSSS, may not be conveyed on the same antenna port, which can result in potential differences in their channel state information (CSI). This poses challenges in the design of coherent NSSS detection methods. Consequently, an NB-IoT UE requires a simple yet robust synchronization technique capable of supporting battery lifetimes exceeding 10 years, especially in regions with poor coverage. Addressing this need, developing a high-performance and still computationally efficient cell search method suitable for the NB-IoT system becomes crucial and challenging.

1.3. Contributions

This paper suggests an efficient joint PCID and CFO synchronization scheme for cellular IoT applications. The proposed NSSS synchronization approach employs a blockwise correlation of NSSS sequences to simultaneously estimate the PCID and CFO in a decoupled manner. The advantage of utilizing the same correlation function for PCID detection is that

it allows for the simultaneous estimation of the CFO, leading to a simpler design for the synchronization receiver. The feasibility of the proposed PCID and CFO synchronization receiver is evidenced by deriving analytical expressions for the detection probability and mean squared error (MSE). Numerical examples demonstrate that the proposed NSSS synchronization method achieves accurate parameter estimates while maintaining relatively lower complexity compared with benchmark methods.

The remainder of this paper is organized as follows. The next section introduces related works on the initial cell search method. Section 3 provides a concise outline of the signal model and SSs for the NB-IoT system. Section 4 presents an enhanced NSSS synchronization scheme, and the detection probability and MSE for the proposed scheme are numerically derived. Section 5 offers a comprehensive presentation of simulation results, evaluating the effectiveness of the presented NSSS detector. Finally, the paper is summarized in Section 6. Table 1 summarizes the notations used in the paper.

Table 1. Main notations used in this paper.

Notation	Description
a^*	Complex conjugation of a complex number a
$\|a\|$	Absolute value of a complex number a
$\angle\{a\}$	Angle of a complex number a
$\Re\{a\}$	Real component of a complex number a
$\Im\{a\}$	Imaginary component of a complex number a
$\lfloor a \rfloor$	Rounding-down operation of variable a
$\lceil a \rceil$	Operation that converts a to the nearest integer
$\mathbb{E}\{a\}$	Expected value of a parameter a
$\hat{a}$	Estimate of a parameter a
$\tilde{a}$	Trial value of a parameter a
$\mathrm{mod}(a, b)$	Modulus operation that returns the integer remainder of a/b
$\tan^{-1}(a)$	Inverse tangent function of a real number a
$G \sim \mathcal{G}(a, b)$	Random variable G is normal, distributed with mean a and variance b

2. Related Works

The initial cell search involves a series of procedures aimed at achieving timing alignment and retrieving the PCID of the eNodeB. This process is divided into three distinct stages. In the first stage, the NPSS is used to assist the UE in estimating STO and CFO, which is accomplished in the time domain [14,15]. In an attempt to expedite the detection process, a full-rate autocorrelation technique is utilized [14]. However, extending the autocorrelation window beyond one subframe results in the NPSS detection location becoming less distinct. In the work presented in [15], the application of a fractional CFO (FCFO) pre-estimator and a noise canceller serves to enhance the accuracy of NPSS detection. With the completion of this step, the processes of timing synchronization and CFO recovery have been successfully carried out. Subsequently, the time-sampled orthogonal frequency division multiplexing (OFDM) signal is transformed to the frequency domain using FFT. In the following stage, the NSSS is employed to establish complete downlink synchronization, enabling the UE to obtain both the PCID and timing with a margin of uncertainty of 80 ms [14–16].

2.1. PCID Detection

Based on the maximum likelihood (ML) principle, the process of obtaining the PCID involves combining four complementary sequences and frame number terms into reconstructed complementary sequences [14,15]. Although the approaches studied in [14,15] offer the benefit of reduced complexity, they rely on cross-correlation and no longer utilize the features of the NSSS to facilitate PCID estimation. The detection strategies introduced in [15,16], on the other hand, exploit the inherent characteristics of the NSSS sequence, resulting in a considerable decrease in computational load when compared with the method in [12]. However, a notable drawback of these noncoherent estimation approaches is their reduced capability to effectively handle the frequency selectivity of the channel. In [16],

a complexity-efficient method for detecting the NSSS using FFT was introduced, intended for scenarios encompassing both unknown and estimated channels. Nevertheless, to mitigate the impact of frequency-selective fading, the adoption of coherent detection methods results in a substantial computational burden during the channel estimation phase. In [17], a detection scheme with reduced complexity was introduced, utilizing the autocorrelation metric rather than cross-correlation. This method leverages the inherent symmetric feature of the NSSS sequence. However, such an advantage is gained at the cost of sacrificing detection performance. In [18], a coherent method for detecting the NSSS was introduced, efficiently decoupling the joint search space of PCID detection into a smaller set of hypotheses. Due to decoupled search space, this approach considerably reduces the number of arithmetic operations required for PCID detection while providing detection capability that is nearly equivalent to those described in [16]. Similar to the approach in [16], there exists a challenge of increased complexity in estimating frequency-selective channels. To simultaneously address issues of performance degradation and complexity, the proposed PCID detection method employs blockwise correlation, eliminating the need for channel estimation while also achieving performance enhancement. Table 2 provides a comparison between previous research studies and the proposed study.

Table 2. Comparison of the solution methods of NSSS detection.

Method	Detection Strategy	Cost Function	RCFO Estimation	Complexity
Ref. [14]	Noncoherent	Cross-correlation	Additional metric required	Medium
Ref. [15]	Noncoherent	Cross-correlation	Additional metric required	Low
Ref. [16]	Coherent/noncoherent	Cross-correlation	Not suggested	High
Ref. [17]	Noncoherent	Autocorrelation	Not suggested	Low
Ref. [18]	Coherent	Cross-correlation	Not suggested	Medium
Proposed	Noncoherent	Cross-correlation	Same correlation metric used	Low

2.2. RCFO Estimation

Upon successfully completing these operations, the UE can access important system information conveyed through a narrowband physical broadcasting channel (NPBCH). For the successful decoding of NPBCH, the frequency offset also needs to be detected and removed [14,15]. Moreover, frequency tracking becomes crucial for NB-IoT systems, as a residual CFO (RCFO) persists even after CFO compensation and continuous frequency drift is introduced by inexpensive oscillators. Taking into account the precision of frequency estimation required in NB-IoT applications, the ML frequency detection strategy developed in [10] is not suitable for the purpose of frequency tracking. To address this issue, the NPSS, NSSS, and NPBCH are jointly utilized to detect the RCFO [15]. Considering the trade-off between complexity and accuracy, the number of correlation pairs can be adjusted according to SNR conditions. For this purpose, a new metric has to be devised, distinct from the one employed for NSSS detection, which leads to an additional increase in complexity. On the contrary, the proposed RCFO estimation scheme offers the advantage of simultaneously estimating the RCFO by utilizing the same metric employed for PCID detection, without introducing an extra increase in complexity.

3. System Description

3.1. Signal Model

We adopt an OFDM system that has N equiwidth subcarriers. By performing an N-point inverse FFT on the frequency-domain (FD) complex data symbol $X_l(m)$ with

symbol energy $E_X = \mathbb{E}\{|X_q(m)|^2\}$ $(m = 0, 1, \cdots, N-1)$, an OFDM symbol is formed and consists of N complex time-domain (TD) samples. To guarantee intersymbol interference-free reception over multipath channels, a cyclic prefix (CP) of duration T_g is inserted between OFDM symbols. By combining these parameters, the resulting OFDM symbol has a duration of $T_u = (N + N_g)T_s = (1 + \rho_1)/\Delta_f$, where T_s is the amount of time between consecutive output samples, N_g is the length of CP, $\rho_1 = N_g/N$, and Δ_f is the subcarrier spacing. Hence, the TD modulated signal at the l-th symbol duration can be expressed as

$$x_l(q) = \sum_{m=0}^{N-1} X_l(m) e^{j2\pi mq/N} \tag{1}$$

where $q = -N_g, -N_g + 1, \cdots, N-1$.

The transmitted signal undergoes propagation through a wireless fading channel and is subject to the presence of additive white Gaussian noise (AWGN). Upon reception, the radio frequency signal centered at f_c is converted to the baseband frequency using the local oscillator frequency $f_c^{'}$. Following this downconversion process, the TD sampled signal is given by

$$y_l(q) = e^{j2\pi l\epsilon\rho_2} e^{j2\pi\epsilon(q-\theta)/N} \sum_{p=1}^{N_r} h_l(p) x_l(q - \tau_p - \theta) + z_l(q) \tag{2}$$

where $q = -N_g, -N_g + 1, \cdots, N-1$, $\rho_2 = 1 + \rho_1$, θ denotes the initial STO, $h_l(p)$ represents the discrete channel impulse response, N_r is the number of multipath replicas, τ_p is the delay of the p-th path, $z_l(q)$ is the zero-mean AWGN with variance σ_z^2, and $\epsilon = (f_c - f_c^{'})/\Delta_f$. It is important to observe that the normalized CFO ϵ can be separated into an integer CFO (ICFO) ϵ_i and an FCFO ϵ_f, resulting in $\epsilon = \epsilon_i + \epsilon_f$.

In the time domain, the receiver is required to detect initial STO and CFO by extracting information from the received signal [14,15]. Consequently, the estimated STO $\hat{\theta}$ and estimated CFO $\hat{\epsilon}$ are acquired during this phase. Even after compensating for these offsets, residual CFO (RCFO) and residual STO (RSTO) remain, defined as $\varepsilon = \epsilon - \hat{\epsilon}$ and $\eta = \theta - \hat{\theta}$, respectively. After removing CP, the received signal undergoes conversion to the frequency domain through the FFT unit. Accordingly, the demodulated FD symbol takes the expression [19]

$$Y_l(m) \approx H_l(m) X_l(m) e^{-j2\pi m\eta/N} e^{j2\pi\varepsilon(l\rho_2+\rho_1)} + I_l(m) + Z_l(m) \tag{3}$$

where $H_l(m)$ represents the CSI following the complex Gaussian distribution $\mathcal{G}(0, \sigma_H^2)$, $I_l(m)$ is the intercarrier interference (ICI) with variance $\sigma_I^2 \approx \mathbb{E}|X_l(m)|^2 \sigma_H^2 \varepsilon^2 \pi^2/3$ during the post-FFT step, and $Z_l(m)$ is the AWGN term having $Z_l(v) \sim \mathcal{G}(0, \sigma_Z^2)$.

3.2. Synchronization Signal

The NB-IoT radio frames are cyclically repeated, totaling 1024 frames. In the time domain, every frame is made up of 10 subframes, with each subframe containing two slots, each lasting for 0.5 ms. Unlike LTE, NB-IoT does not allow an extended CP, so 7 OFDM symbols are combined into one slot. In the frequency domain, each OFDM symbol comprises 12 subcarriers, occupying a bandwidth of 180 kHz. For the purpose of identifying any available eNodeB, NB-IoT utilizes two types of signals: narrowband reference signals and SSs. The former is exclusively used for estimating the CSI, whereas the latter, namely, the NPSS and NSSS, serves the purpose of establishing the connection between eNodeB and UE. Specifically, the NPSS is employed for the purpose of assisting the UE in estimating time and frequency offsets, whereas the NSSS serves to achieve full downlink synchronization, allowing the UE to obtain the PCID and timing with an uncertainty of 80 ms.

The process of generating the SS sequences involves deriving the NPSS and NSSS from ZC sequences [20]. The NPSS is intentionally designed to withstand the influence of significant CFO and is created by performing subcarrier-wise multiplication between a ZC sequence and a binary cover code. The formulation can be described as

$$W_l(m) = B_l e^{-j5\pi m(m+1)/11},\ 0 \le m < 12, 3 \le l < 14 \tag{4}$$

where the binary cover code $B_l = \{1, 1, 1, 1, -1, -1, 1, 1, 1, -1, 1\}$ is of size 11 and extends across the last 11 OFDM symbols. This code remains constant for all values of l and does not carry any cell-specific information. In each fifth subframe, the sequence $W_l(m)$ is consistently positioned within the last 11 OFDM symbols, resulting in a total of 132 resource elements (REs). Each RE corresponds to a resource block (RB) comprising 12 subcarriers. To simplify NPSS detection and reduce computational complexity, the NPSS remains fixed for each subframe. Consequently, NB-IoT UEs only need to identify for a single NPSS during their operation.

The NSSS is created through the element-wise multiplication of a ZC sequence and a binary Hadamard–Walsh sequence, resulting in the expression $c_n(g')e^{-j\pi w g''(g''+1)/131}$, where $n = \lfloor v/126 \rfloor$, $w = \mathrm{mod}(v, 126) + 3$, $g' = \mathrm{mod}(g, 128)$, and $g'' = \mathrm{mod}(g, 131)$ for $0 \le g < 132$. It is important to note that the PCID, denoted as v, determines the root of both the ZC sequence and binary Hadamard–Walsh sequence. To complete the construction of the NSSS, the cyclic shift of the ZC sequence undergoes additional scrambling by the radio frame number (RFN). Considering these notations, a PCID v has a relationship with the variables w and n, where $v = w - 3 + 126n$. Accordingly, the NSSS can be formulated as

$$C(g) = c_n(g')e^{-j2\pi ug}e^{-j\pi w g''(g''+1)/131},\ 0 \le g < 132 \tag{5}$$

where $v \in \{0, 1, 2, \cdots, 503\}$ stands for the PCID and the value of u is determined based on the RFN n_r. By taking length-128 Hadamard–Walsh sequences and cyclically appending the first four components, the sequence $c_n(g')$ is extended to form a length-132 sequence [5]. NB-IoT supports a total of 504 distinct PCIDs, each associated with the NSSS. During every even frame, each PCID is transmitted with four unique phase shifts, which serves to indicate 80 ms frame boundaries.

To simplify the explanation, we group $C(g)$ into equisized 11 sub-blocks, and each sub-block is subsequently allocated to 11 OFDM symbols. Consequently, the transmission bandwidth for both SSs occupies only one RB. With this notation, let us define the l-th symbol at the m-th subcarrier as $C_l^{n,u,w}(m)$, where $3 \le l \le 13$ and $0 \le m < 12$. The mapping from $C(g)$ to $C_l^{n,u,w}(m)$ is carried out by first sorting in ascending order of the index m, followed by the index l.

3.3. Cell Search Procedure

Typically, the initial cell search procedure involves both TD and FD processing [15]. The first step in the time domain is to detect coarse STO and FCFO using the autocorrelation function. After coarse STO and FCFO are detected and recovered from (2), the joint detection of the ICFO and fine STO is essential, typically accomplishedly employing the cross-correlation function. Once these ambiguities have been successfully resolved in the pre-FFT step, the UE proceeds to detect the PCID and to track the RCFO. The PCID and RCFO can be jointly detected in the frequency domain.

4. Proposed Joint PCID and CFO Detection Method

This section presents an effective formulation for joint PCID and RCFO detection in the cellular IoT system and verifies the detection capability of the proposed method by deriving the detection probability and MSE as performance measures.

4.1. Algorithm Description

Under the assumption that the channel remains relatively stable during one NSSS sequence, considering a low mobility UE, the detection of NSSS is carried out on a block-by-block basis. However, the simulation section will address the influence of Doppler frequency on the synchronization performance. Let the size of the first block be denoted as N_b, which comprises a set of successive observation symbols. Given that the estimation scheme relies on observing a single NSSS sequence assigned to 11 OFDM symbols, the size of the second block is then determined as $11 - N_b$. With this formulation at hand, the proposed cost function can be described as

$$\Omega(\tilde{n},\tilde{u},\tilde{w}) = \sum_{m\in\mathcal{S}} \left\{ \sum_{l_1=3}^{N_b+2} \bar{Y}_{l_1}^{\tilde{n},\tilde{u},\tilde{w}}(m) \right\}^* \sum_{l_2=N_b+3}^{13} \bar{Y}_{l_2}^{\tilde{n},\tilde{u},\tilde{w}}(m) \tag{6}$$

where $\mathcal{S} = \{m | 0 \le m < 12\}$ stands for the set of NSSS subcarrier index, $\tilde{n} \in \{0,1,2,3\}$ denotes the hypothetical value of n, $\tilde{u} \in \{0,1/4,2/4,3/4\}$ denotes the hypothetical value of u, $\tilde{w} \in \{3,4,\cdots,128\}$ denotes the hypothetical value of w, and $\bar{Y}_l^{\tilde{n},\tilde{u},\tilde{w}}(m) = Y_l(m)C_l^{\tilde{n},\tilde{u},\tilde{w}*}(m)$. Based on the assumption that the channel is static during NSSS block, the cost function can be represented by

$$\begin{aligned}\Omega(\tilde{n},\tilde{u},\tilde{w}) = \sum_{m\in\mathcal{S}} |H_l(m)|^2 \sum_{l_1=3}^{N_b+2} \bar{X}_{l_1}^{\tilde{n},\tilde{u},\tilde{w}*}(m) \sum_{l_2=N_b+3}^{13} \bar{X}_{l_2}^{\tilde{n},\tilde{u},\tilde{w}}(m) e^{j2\pi\rho_2\varepsilon(l_2-l_1)} \\ + \sum_{m\in\mathcal{S}} \bar{I}(m) + \sum_{m\in\mathcal{S}} \bar{Z}(m)\end{aligned} \tag{7}$$

where $\bar{X}_l^{\tilde{n},\tilde{u},\tilde{w}}(m) = X_l(m)C_l^{\tilde{n},\tilde{u},\tilde{w}*}(m)$ is the NSSS-compensated transmitted signal. In (7), the noise contributions $\bar{I}(m)$ and $\bar{Z}(m)$ are respectively given by

$$\bar{I}(m) = \sum_{l_1=3}^{N_b+2} \sum_{l_2=N_b+3}^{13} \bar{I}_{l_1,l_2}(m)\bar{C}_{l_1,l_2}^{\tilde{n},\tilde{u},\tilde{w}}(m) \tag{8}$$

and

$$\bar{Z}(m) = \sum_{l_1=3}^{N_b+2} \sum_{l_2=N_b+3}^{13} \bar{Z}_{l_1,l_2}(m)\bar{C}_{l_1,l_2}^{\tilde{n},\tilde{u},\tilde{w}}(m) \tag{9}$$

where $\bar{I}_{l_1,l_2}(m) = H_{l_1}^*(m)\bar{X}_{l_1}^*(m)I_{l_2}(m)e^{-j2\pi\varepsilon(l_2\rho_2+\rho_1)} + H_{l_2}(m)\bar{X}_{l_2}(m)I_{l_1}^*(m)e^{j2\pi\varepsilon(l_1\rho_2+\rho_1)} + I_{l_2}(m)Z_{l_1}^*(m) + I_{l_1}^*(m)Z_{l_2}(m) + I_{l_1}^*(m)I_{l_2}(m)$, $\bar{Z}_{l_1,l_2}(m) = H_{l_1}^*(m)\bar{X}_{l_1}^*(m)Z_{l_2}(m)e^{-j2\pi\varepsilon(l_1\rho_2+\rho_1)} + H_{l_2}(m)\bar{X}_{l_2}(m)Z_{l_1}^*(m)e^{j2\pi\varepsilon(l_2\rho_2+\rho_1)} + Z_{l_1}^*(m)Z_{l_2}(m)$, and $\bar{C}_{l_1,l_2}^{\tilde{n},\tilde{u},\tilde{w}}(m) = C_{l_1}^{\tilde{n},\tilde{u},\tilde{w}}(m)C_{l_2}^{\tilde{n},\tilde{u},\tilde{w}*}(m)$. Note that $\bar{X}_{l_1}^{\tilde{n},\tilde{u},\tilde{w}*}(m)\bar{X}_{l_2}^{\tilde{n},\tilde{u},\tilde{w}}(m) = E_X^2$ for $(\tilde{n},\tilde{u},\tilde{w}) = (n,u,w)$, while $\bar{X}_{l_1}^{\tilde{n},\tilde{u},\tilde{w}*}(m)\bar{X}_{l_2}^{\tilde{n},\tilde{u},\tilde{w}}(m)$ is a complex random sequence for $(\tilde{n},\tilde{u},\tilde{w}) \neq (n,u,w)$.

If we assume that the hypothesized values $(\tilde{n},\tilde{u},\tilde{w})$ exactly match with the actual values (n,u,w), i.e., hypothesis H_1, it is seen that $\bar{X}_{l_1}^{\tilde{n},\tilde{u},\tilde{w}*}(m)\bar{X}_{l_2}^{\tilde{n},\tilde{u},\tilde{w}}(m) = E_X^2$, and thus, one obtains

$$\Omega(\tilde{n},\tilde{u},\tilde{w}) = E_X^2 \sum_{m\in\mathcal{S}} |H_l(m)|^2 \sum_{l_1=3}^{N_b+2} \sum_{l_2=N_b+3}^{13} e^{j2\pi\rho_2\varepsilon(l_2-l_1)} + \sum_{m\in\mathcal{S}} \bar{I}(m) + \sum_{m\in\mathcal{S}} \bar{Z}(m) \tag{10}$$

where some of the terms on the right-hand side are further derived as follows:

$$\sum_{l_1=3}^{N_b+2} \sum_{l_2=N_b+3}^{13} e^{j2\pi\rho_2\varepsilon(l_2-l_1)} = \underbrace{\frac{\sin(\pi\varepsilon(11-N_b)\rho_2)}{\sin(\pi\varepsilon\rho_2)} \frac{\sin(-\pi\varepsilon N_b\rho_2)}{\sin(-\pi\varepsilon\rho_2)}}_{f_1(\varepsilon,N_b)} e^{j11\pi\varepsilon\rho_2}. \tag{11}$$

For typical values of ε, $f_1(\varepsilon, N_b) \approx (11 - N_b)N_b$, and it depends on only the block size N_b. In this case, $\Omega(\tilde{n}, \tilde{u}, \tilde{w})$ is simplified to

$$\Omega(\tilde{n}, \tilde{u}, \tilde{w}) \approx (11 - N_b)N_b E_X^2 e^{j11\pi\varepsilon\rho_2} \sum_{m\in\mathcal{S}} |H_l(m)|^2 + \sum_{m\in\mathcal{S}} \bar{I}(m) + \sum_{m\in\mathcal{S}} \bar{Z}(m). \tag{12}$$

Using an approximate ML (AML) approach [21], the NSSS and RCFO are jointly estimated as

$$(\hat{n}, \hat{u}, \hat{w}, \hat{\varepsilon}) = \underset{(\tilde{n},\tilde{u},\tilde{w},\tilde{\varepsilon})}{\arg\max}\, \Re\{\Omega(\tilde{n}, \tilde{u}, \tilde{w})e^{-j11\pi\tilde{\varepsilon}\rho_2}\}. \tag{13}$$

For each trial value of $(\tilde{n}, \tilde{u}, \tilde{w})$, the AML estimator performs an exhaustive search of ε by appropriately quantizing the possible values of RCFO, which undertakes significant arithmetic complexity. To address this problem, the search process is simplified from a two-dimensional search of (n, u, w, ε) to a one-dimensional search for (n, u, w), along with a separate one-dimensional search for ε. Figure 1 illustrates the block diagram of the overall cell search process containing the identification of both NPSS and NSSS. The main focus of this paper is on joint detection of the PCID and RCFO utilizing the NSSS.

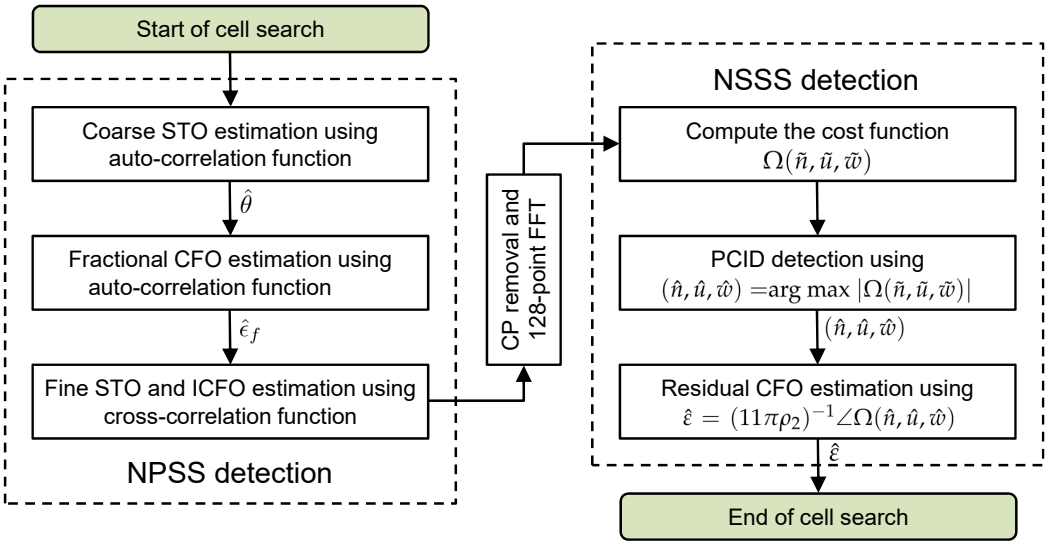

Figure 1. Block diagram of the overall cell search process for NB-IoT.

In order to find a maximum of the cost function $\Re\{\Omega(\tilde{n}, \tilde{u}, \tilde{w})e^{-j11\pi\varepsilon\rho_2}\}$ with respect to (n, u, w, ε), it is necessary that $\angle\{\Omega(\tilde{n}, \tilde{u}, \tilde{w})e^{-j11\pi\varepsilon\rho_2}\} = \angle\{\Omega(\tilde{n}, \tilde{u}, \tilde{w})\} - 11\pi\varepsilon\rho_2 = 0$ in (13). Therefore, setting $\angle\Omega(\tilde{n}, \tilde{u}, \tilde{w}) = 11\pi\varepsilon\rho_2$ to be zero removes the imaginary part of $\Omega(\tilde{n}, \tilde{u}, \tilde{w})e^{-j11\pi\varepsilon\rho_2}$, so this is a necessary condition for $\Re\{\Omega(\tilde{n}, \tilde{u}, \tilde{w})e^{-j11\pi\varepsilon\rho_2}\}$ to be maximum. Therefore, the RCFO estimation is formulated as follows:

$$\hat{\varepsilon} = \frac{1}{11\pi\rho_2}\angle\Omega(\tilde{n}, \tilde{u}, \tilde{w}). \tag{14}$$

Recalling from (12) that $e^{-j11\pi\hat{\varepsilon}\rho_2} = \Omega^*(\tilde{n}, \tilde{u}, \tilde{w})/|\Omega(\tilde{n}, \tilde{u}, \tilde{w})|$, the cost function can be rewritten as $\Omega(\tilde{n}, \tilde{u}, \tilde{w}) = |\Omega(\tilde{n}, \tilde{u}, \tilde{w})|e^{j11\pi\hat{\varepsilon}\rho_2}$. Substituting it back into (13), we observe that the quantity $\Re\{\Omega(\tilde{n}, \tilde{u}, \tilde{w})e^{-j11\pi\hat{\varepsilon}\rho_2}\}$ is reduced to $|\Omega(\tilde{n}, \tilde{u}, \tilde{w})|$ if $\varepsilon = \hat{\varepsilon}$, which allows for detecting the NSSS and RCFO in a decoupled fashion. Consequently, (n, u, w) can be first estimated as

$$(\hat{n}, \hat{u}, \hat{w}) = \underset{(\tilde{n},\tilde{u},\tilde{w})}{\arg\max}\, |\Omega(\tilde{n}, \tilde{u}, \tilde{w})| \tag{15}$$

and $(\hat{n}, \hat{u}, \hat{w})$ are then plugged into (14), eventually yielding $\hat{\varepsilon} = (11\pi\rho_2)^{-1}\angle\Omega(\hat{n}, \hat{u}, \hat{w})$. Using (15), the detection of the PCID v is performed, resulting in $\hat{v} = \hat{w} - 3 + 126\hat{n}$.

4.2. Performance Analysis

In order to assess the performance of the PCID and RCFO estimation method, we derive the detection probability of the PCID detector and the MSE of the RCFO estimator in a flat-fading channel. Because this paper focuses on NSSS detection, it is assumed that the ICFO and STO have been accurately estimated using the NPSS.

4.2.1. PCID Detection

The detection probability of (15) is derived, assuming a flat-fading condition. The detection probability is the probability that (n, u, w) are erroneously detected and is denoted as $P_d = \text{Prob}\{(\hat{n}, \hat{u}, \hat{w}) = (n, u, w)\}$. When $(\tilde{n}, \tilde{u}, \tilde{w}) = (n, u, w)$ (hypothesis H_1), conditioned on $\beta = |H_l(m)|^2$, $\Omega(\tilde{n}, \tilde{u}, \tilde{w})e^{-j11\pi\hat{\varepsilon}\rho_2} \sim \mathcal{G}(\mu, \sigma_1^2)$ with $\mu = 12(11 - N_b)N_b E_X^2\beta$ and $\sigma_1^2 \approx 12(\sigma_{\bar{I}}^2 + \sigma_{\bar{Z}}^2)$, where $\sigma_{\bar{I}}^2$ and $\sigma_{\bar{Z}}^2$ denote variances of $\bar{I}(m)$ and $\bar{Z}(m)$, respectively. It is easily seen from (8) and (9) that $\sigma_{\bar{I}}^2 = (11 - N_b)N_b E_X^2(2E_X\sigma_I^2\beta + 2\sigma_I^2\sigma_Z^2 + \sigma_I^4)$ and $\sigma_{\bar{Z}}^2 = (11 - N_b)N_b E_X^2(2E_X\sigma_Z^2\beta + \sigma_Z^4)$. In hypothesis H_1, therefore, the probability density function (PDF) of $z = |\Omega(\tilde{n}, \tilde{u}, \tilde{w})e^{-j11\pi\hat{\varepsilon}\rho_2}| = |\Omega(\tilde{n}, \tilde{u}, \tilde{w})|$ in (15) follows the Rician distribution, i.e.,

$$f_{H_1}(z) = \frac{2z}{\sigma_1^2} e^{-\frac{z^2+\mu^2}{\sigma_1^2}} I_0\left(\frac{2z\mu}{\sigma_1^2}\right) \tag{16}$$

where the function $I_0(x)$ represents the modified Bessel function of the first kind with a zeroth order. Under hypothesis H_0, i.e., $(\tilde{n}, \tilde{u}, \tilde{w}) \neq (n, u, w)$, we have $\Omega(\tilde{n}, \tilde{u}, \tilde{w})e^{-j11\pi\hat{\varepsilon}\rho_2} \sim \mathcal{G}(0, \sigma_0^2)$ with $\sigma_0^2 \approx 12(11 - N_b)N_b E_X^4\beta^2 + \sigma_1^2$. In this null hypothesis, the PDF of $|\Omega(\tilde{n}, \tilde{u}, \tilde{w})|$ is expressed as $f_{H_0}(z) = 2z/\sigma_0^2 e^{-z^2/\sigma_0^2}$. Thus, making use of two PDFs, the conditional probability that (n, u, w) are erroneously detected given the channel gain β can be defined as

$$\begin{aligned} P_d(\beta) &= \int_0^\infty f_{H_1}(z)\left[\int_0^z f_{H_0}(x)dx\right]^{2015} dz \\ &= \int_0^\infty \frac{2z}{\sigma_1^2} e^{-\frac{z^2+\mu^2}{\sigma_1^2}} I_0\left(\frac{2z\mu}{\sigma_1^2}\right)\left[1 - e^{-\frac{z^2}{\sigma_0^2}}\right]^{2015} dz. \end{aligned} \tag{17}$$

With the use of binomial expansion in (17), $P_d(\beta)$ becomes

$$P_d(\beta) = e^{-\frac{\mu^2}{\sigma_1^2}} \sum_{g=0}^{2015} (-1)^g \binom{2015}{g} \int_0^\infty \frac{2z}{\sigma_1^2} e^{-z^2(1/\sigma_1^2 + g/\sigma_0^2)} I_0\left(\frac{2z\mu}{\sigma_1^2}\right) dz \tag{18}$$

which is further simplified into

$$P_d(\beta) = \sum_{g=0}^{2015} \binom{2015}{g} \frac{(-1)^g}{1 + g\sigma_1^2/\sigma_0^2} e^{-\frac{g}{\sigma_0^2/\mu^2 + g\sigma_1^2/\mu^2}}. \tag{19}$$

It is worth highlighting from (19) that the ratio of mean power to variance of the cost function $\Omega(\tilde{n}, \tilde{u}, \tilde{w})e^{-j11\pi\hat{\varepsilon}\rho_2}$ is expressed as

$$\frac{\sigma_1^2}{\mu^2} = \frac{f_2(\gamma_i, \gamma_z)}{12(11 - N_b)N_b} \tag{20}$$

and

$$\frac{\sigma_0^2}{\mu^2} = \frac{1 + f_2(\gamma_i, \gamma_z)}{12(11 - N_b)N_b} \tag{21}$$

with

$$f_2(\gamma_i, \gamma_z) = \frac{2}{\gamma_i} + \frac{2}{\gamma_z} + \left(\frac{1}{\gamma_i} + \frac{1}{\gamma_z}\right)^2 \tag{22}$$

where $\gamma_i = \beta E_X/\sigma_I^2$ is the instantaneous signal-to-ICI ratio (SIR) and $\gamma_z = \beta E_X/\sigma_Z^2$ is the instantaneous SNR. To obtain unconditional detection probability, we take the average of $P_d(\beta)$ with respect to β, which has a PDF as $f(\beta) = (1/\sigma_H^2)e^{-\beta/\sigma_H^2}$, leading to $P_d = \int_0^\infty P_d(\beta)f(\beta)d\beta$.

Next, we find an optimal value of N_b that offers a maximum detection probability. Since $\sigma_1^2/\sigma_0^2 = f_2(\gamma_i, \gamma_z)/(1 + f_2(\gamma_i, \gamma_z))$ is not a function of N_b, substituting (20) and (21) into (19) leads to

$$P_d(\beta) = \sum_{g=0}^{2015} \binom{2015}{g} f_1(g) e^{-\frac{(11-N_b)N_b}{f_2(g)}} \tag{23}$$

where the two quantities $f_1(g) = (-1)^g/(1 + gf_2(\gamma_i, \gamma_z)/(1 + f_2(\gamma_i, \gamma_z)))$ and $f_2(g) = f_2(\gamma_i, \gamma_z)/g + f_2(\gamma_i, \gamma_z) + 1$ do not resort to the parameter N_b. By differentiating (23) with respect to N_b and setting it to zero, one can easily find a value of N_b, which maximizes (23), eventually yielding

$$(11 - 2N_b) \sum_{g=0}^{2015} \binom{2015}{g} f_1(g) f_2(g) e^{-\frac{(11-N_b)N_b}{f_2(g)}} = 0 \tag{24}$$

which informs us that only a single solution is equal to $N_b = 11/2$. As N_b is an integer-valued design parameter, it can be expressed as $N_b = \lfloor 11/2 \rceil$. Therefore, the optimal detection probability of the proposed PCID detector can be obtained as

$$P_d(\beta) = \sum_{g=0}^{2015} \binom{2015}{g} (-1)^g \left(1 + \frac{g f_2(\gamma_i, \gamma_z)}{1 + f_2(\gamma_i, \gamma_z)}\right)^{-1} e^{-\frac{(11-\lfloor 11/2 \rceil)\lfloor 11/2 \rceil}{f_2(\gamma_i,\gamma_z)/g + f_2(\gamma_i,\gamma_z)+1}}. \tag{25}$$

4.2.2. RCFO Estimation

The MSE of (14) is derived under a time-invariant flat-fading condition, supposing that $(\hat{n}, \hat{u}, \hat{w}) = (n, u, w)$ at the UE terminal. Letting $\hat{\Omega}(\tilde{n}, \tilde{u}, \tilde{w}) = \Omega(\tilde{n}, \tilde{u}, \tilde{w})e^{-j11\pi\varepsilon\rho_2}$, (12) can be rearranged into

$$\hat{\Omega}(\tilde{n}, \tilde{u}, \tilde{w}) = (11 - N_b)N_b E_X^2 \sum_{m \in \mathcal{S}} |H_l(m)|^2 \left[1 + \frac{\sum_{m \in \mathcal{S}} \hat{I}(m) + \sum_{m \in \mathcal{S}} \hat{Z}(m)}{(11 - N_b)N_b E_X^2 \sum_{m \in \mathcal{S}} |H_l(m)|^2}\right] \tag{26}$$

where $\hat{I}(m) = \bar{I}(m)e^{-j11\pi\varepsilon\rho_2}$ and $\hat{Z}(m) = \bar{Z}(m)e^{-j11\pi\varepsilon\rho_2}$. For SNR $\gg 1$, it is safe to assume that $\Re\{\sum_{m \in \mathcal{S}} \hat{I}(m) + \sum_{m \in \mathcal{S}} \hat{Z}(m)\}/((11 - N_b)N_b E_X^2 \sum_{m \in \mathcal{S}} |H_l(m)|^2) \ll 1$. Based on this assumption, we consequently state that

$$\begin{aligned} \angle\hat{\Omega}(\tilde{n}, \tilde{u}, \tilde{w}) &= \angle\left[1 + \frac{\sum_{m \in \mathcal{S}} \hat{I}(m) + \sum_{m \in \mathcal{S}} \hat{Z}(m)}{(11 - N_b)N_b E_X^2 \sum_{m \in \mathcal{S}} |H_l(m)|^2}\right] \\ &= \angle e^{j \tan^{-1}\left(\frac{\sum_{m \in \mathcal{S}} \Im\{\hat{I}(m)\} + \sum_{m \in \mathcal{S}} \Im\{\hat{Z}(m)\}}{(11-N_b)N_b E_X^2 \sum_{m \in \mathcal{S}} |H_l(m)|^2}\right)}. \end{aligned} \tag{27}$$

Since $\angle\hat{\Omega}(\tilde{n},\tilde{u},\tilde{w}) = \angle\Omega(\tilde{n},\tilde{u},\tilde{w}) - 11\pi\varepsilon\rho_2$, assuming that $\Delta_\varepsilon = \hat{\varepsilon} - \varepsilon$ is negligible and $\angle e^{j\tan^{-1}(z)} \approx \angle e^{jz} = z$ for high SNR regime, it follows that

$$\Delta_\varepsilon \approx \frac{1}{11\pi\rho_2} \frac{\sum_{m\in\mathcal{S}} \Im\{\hat{I}(m)\} + \sum_{m\in\mathcal{S}} \Im\{\hat{Z}(m)\}}{12(11-N_b)N_b E_X^2 \beta}. \tag{28}$$

Since $\bar{I}(m)$ and $\bar{Z}(m)$ are statistically identical to $\hat{I}(m)$ and $\hat{Z}(m)$, respectively, it is effortlessly seen from (28) that $\mathbb{E}\{\Im\{\hat{I}(m)\}\} = \mathbb{E}\{\Im\{\hat{Z}(m)\}\} = 0$, and thus, the MSE of (14) is described as

$$\begin{aligned}\mathbb{E}\{|\Delta_\varepsilon|^2\} = &\left(\frac{1}{132\pi\rho_2(11-N_b)N_b}\right)^2 \sum_{m\in\mathcal{S}} \mathbb{E}\left\{\left|\frac{\Im\{\hat{I}(m)\}}{E_X^2\beta}\right|^2\right\} \\ &+ \left(\frac{1}{132\pi\rho_2(11-N_b)N_b}\right)^2 \sum_{m\in\mathcal{S}} \mathbb{E}\left\{\left|\frac{\Im\{\hat{Z}(m)\}}{E_X^2\beta}\right|^2\right\}\end{aligned} \tag{29}$$

where

$$\mathbb{E}\left\{\left|\frac{\Im\{\hat{I}(m)\}}{E_X^2\beta}\right|^2\right\} = (11-N_b)N_b\left(\frac{1}{\gamma_i} + \frac{1}{\gamma_i\gamma_z} + \frac{1}{2\gamma_i^2}\right) \tag{30}$$

and

$$\mathbb{E}\left\{\left|\frac{\Im\{\hat{Z}(m)\}}{E_X^2\beta}\right|^2\right\} = (11-N_b)N_b\left(\frac{1}{\gamma_z} + \frac{1}{2\gamma_z^2}\right). \tag{31}$$

Using (29)–(31), after simple manipulations, $\mathbb{E}\{|\Delta_\varepsilon|^2\}$ can be computed as

$$\mathbb{E}\{|\Delta_\varepsilon|^2\} = \frac{f_2(\gamma_i,\gamma_z)}{1452\pi^2\rho_2^2(11-N_b)N_b}. \tag{32}$$

To obtain an optimal N_b, which minimizes $\mathbb{E}\{|\Delta_\varepsilon|^2\}$, we similarly take the derivative of (32) with respect to N_b and make it equal to zero. Hence, we have

$$\frac{(11-2N_b)f_2(\gamma_i,\gamma_z)}{1452\pi^2\rho_2^2(11-N_b)^2N_b^2} = 0. \tag{33}$$

Since $f_2(\gamma_i,\gamma_z)$ is not a function of N_b and $1 \le N_b \le 10$, it is readily seen that $N_b = 11/2$, which is consistent with the result of (24). Similarly, the minimum MSE can be obtained as

$$\mathbb{E}\{|\Delta_\varepsilon|^2\} = \frac{1}{1452\pi^2\rho_2^2(11-\lfloor 11/2\rceil)\lfloor 11/2\rceil}\left[\frac{2}{\gamma_i} + \frac{2}{\gamma_z} + \left(\frac{1}{\gamma_i} + \frac{1}{\gamma_z}\right)^2\right]. \tag{34}$$

5. Numerical Results and Analysis

To evaluate the viability of the proposed NSSS synchronization method, we conduct simulations and perform a comprehensive comparison with conventional synchronization methods using Matlab software. We examine the trade-off between the detection capability and the arithmetic burden of the proposed NSSS detection method.

5.1. Simulation Setup

Our focus is on the NB-IoT system, which operates within a transmission bandwidth of 180 kHz in the 900 MHz band. According to the NB-IoT specification [5], the system

is configured with an FFT size of $N = 128$ and a CP length of $N_g = 10$, resulting in a total symbol duration of 138. Under the given conditions, the sampling time period is $T_s = 0.52$ µs, the subcarrier spacing is $\Delta_f = 15$ kHz, and the number of the NSSS samples is $N_s = 132$. In our simulation, we evaluate the efficiency of the proposed approach by employing two representative channels, namely, the pedestrian and vehicular channel models, as mentioned in [22]. The maximum delay spreads in pedestrian and vehicular channel models are 0.41 and 2.15 µs, respectively. Taking into account the typically low mobility of NB-IoT UEs, we assume a maximum Doppler frequency of 1 Hz for the simulated pedestrian channel [15,23]. For the vehicular scenario, we conduct simulations with a Doppler frequency of 55 Hz, representing a maximum UE speed of 60 km/h [24]. To account for the common oscillator stability of ±20 ppm at the 900 MHz carrier frequency, we consider a maximum CFO uncertainty of ±18 kHz, which enables us to set $\epsilon = 1.2$.

5.2. Benchmark Method

5.2.1. PCID Detection

To confirm the advantages of the proposed PCID synchronization method, we consider three different PCID detection schemes as benchmarks. The first benchmark is a reduced-complexity PCID detection (RPCD) scheme proposed in [15] and uses the following cost function:

$$\Phi_{RPCD}(\tilde{n},\tilde{u},\tilde{w}) = \sum_{l=3}^{13}\sum_{m\in\mathcal{S}} Y_l(m)C_l^{\tilde{n},\tilde{u},\tilde{w}*}(m). \tag{35}$$

Using (35), a joint estimation of (n,u,w) can be formulated by

$$(\hat{n},\hat{u},\hat{w}) = \underset{(\tilde{n},\tilde{u},\tilde{w})}{\arg\max}\, |\Phi_{RPCD}(\tilde{n},\tilde{u},\tilde{w})|. \tag{36}$$

In the case of hypothesis H_1, $|\Phi_{RPCD}(\tilde{n},\tilde{u},\tilde{w})|$ is Rician-distributed with a mean and variance equal to $\mu = \beta N_s E_X$ and $\sigma_1^2 = \beta N_s E_X(\sigma_Z^2+\sigma_I^2)$, respectively. On the other hand, $|\Phi_{RPCD}(\tilde{n},\tilde{u},\tilde{w})|$ is Rayleigh-distributed with a variance equal to $\sigma_0^2 = \beta^2 N_s E_X^2 + \beta N_s E_X(\sigma_Z^2+\sigma_I^2)$ under a null hypothesis. Similarly, the detection probability of the RPCD approach is described as

$$P_d(\beta) = \int_0^\infty 2z(\gamma+1)e^{-(\gamma+1)z^2-N_s\gamma} I_0\left(2z\sqrt{N_s\gamma(\gamma+1)}\right)\left[1-e^{-z^2}\right]^{2015} dz \tag{37}$$

where $\gamma = \gamma_z + \gamma_i$.

The second baseline is a DFT-based PCID detection (DPCD) method developed in [16], which relies on a knowledge of the channel. Denoting the estimated CSI as $H_l(m) = |H_l(m)|e^{j\theta(m)}$, $\theta(m)$ is estimated as

$$\hat{\theta}^{\tilde{n},\tilde{u},\tilde{w}}(m) = \angle\left\{\sum_{l=3}^{13} Y_l(m)C_l^{\tilde{n},\tilde{u},\tilde{w}*}(m)\right\},\ m\in\mathcal{S}. \tag{38}$$

By making use of $\hat{\theta}^{\tilde{n},\tilde{u},\tilde{w}}(m)$ and the cost function in (35) with $Y_l(m)$ replaced by $\hat{Y}_l(m) = Y_l(m)e^{-j\hat{\theta}^{\tilde{n},\tilde{u},\tilde{w}}(m)}$, the DPRD approach coherently estimates the PCID by searching a maximum of $\Re\{\sum_{l=3}^{13}\sum_{m\in\mathcal{S}}\hat{Y}_l(m)C_l^{\tilde{n},\tilde{u},\tilde{w}*}(m))\}$ over $(\tilde{n},\tilde{u},\tilde{w})$. Assuming a perfectly known channel, we have $\Re\{\sum_{l=3}^{13}\sum_{m\in\mathcal{S}}\hat{Y}_l(m)C_l^{\tilde{n},\tilde{u},\tilde{w}*}(m))\} \sim \mathcal{G}(\mu,\sigma_1^2/2)$ under hypothesis H_1, while $\Re\{\sum_{l=3}^{13}\sum_{m\in\mathcal{S}}\hat{Y}_l(m)C_l^{\tilde{n},\tilde{u},\tilde{w}*}(m))\} \sim \mathcal{G}(0,\sigma_0^2/2)$ under hypothesis H_0. Based on this observation, the detection probability of the DPCD approach is given by

$$P_d(\beta) = \int_{-\infty}^{\infty}\frac{1}{\sqrt{2\pi}}e^{-\frac{z^2}{2}}\left[1-Q\left(\frac{z+\sqrt{N_s\gamma}}{\sqrt{\gamma+1}}\right)\right]^{2015} dz \tag{39}$$

where $Q(x)$ is the Q-function.

The last benchmark is a sequential PCID detection (SPCD) method [18], which comprises two steps. In the first stage, the cost function with reduced search space can be described by

$$\begin{aligned}\Re\{\Phi_{SPCS}(\tilde{n},\tilde{u},\tilde{w}')\} = &\sum_{m\in\mathcal{S}}\sum_{l=3}^{13}\Re\{\hat{Y}_l(m)\}\Re\{C_l^{\tilde{n},\tilde{u},\tilde{w}'}(m)\}\\ &+\left|\sum_{m\in\mathcal{S}}\sum_{l=3}^{13}\Im\{\hat{Y}_l(m)\}\Im\{C_l^{\tilde{n},\tilde{u},\tilde{w}'}(m)\}\right|\end{aligned} \tag{40}$$

where $\tilde{w}'$ is the trial value of $w' \in \{3,4,\cdots,65\}$. Then, $(\hat{n},\hat{u},\hat{w}')$ are founded by locating a maximum of $\Re\{\Phi_{SPCS}(\tilde{n},\tilde{u},\tilde{w}')\}$ over $(\tilde{n},\tilde{u},\tilde{w}')$. In the second step, the estimate of w'' is obtained by searching a maximum of $\Re\{\sum_{l=3}^{13}\sum_{m\in\mathcal{S}}\hat{Y}_l(m)C_l^{\hat{n},\hat{u},\tilde{w}''*}(m)\}$ with respect to $\tilde{w}''$, where $\tilde{w}''$ is the trial value of $w'' \in \{\hat{w}', 131-\hat{w}'\}$.

5.2.2. RCFO Estimation

Since the less-expensive oscillator in the NB-IoT UE incurs RCFO and continuous frequency drift, it becomes imperative to track the frequency offset. By using the estimates $(\hat{n},\hat{u},\hat{w})$ obtained through PCID detection, the RCFO estimation method developed in [15] can be effortlessly modified to work with the NSSS, thereby producing the following expression:

$$\hat{\varepsilon} = \frac{1}{2\pi D_t\rho_2}\angle\left\{\sum_{m\in\mathcal{S}}\sum_{l=3}^{13-D_t}\bar{Y}_l^{\hat{n},\hat{u},\hat{w}}(m)\bar{Y}_{l+D_t}^{\hat{n},\hat{u},\hat{w}*}(m)\right\} \tag{41}$$

where $\bar{Y}_l^{\hat{n},\hat{u},\hat{w}}(m) = Y_l(m)C_l^{\hat{n},\hat{u},\hat{w}*}(m)$ is the NSSS-compensated received signal and D_t is the distance between correlation pairs in the time direction. Similarly, the MSE of (41) is computed as

$$\mathbb{E}\{|\Delta_\varepsilon|^2\} = \frac{1}{48\pi^2 D_t^2\rho_2^2(11-D_t)}\left[\frac{2}{\gamma_i}+\frac{2}{\gamma_z}+\left(\frac{1}{\gamma_i}+\frac{1}{\gamma_z}\right)^2\right]. \tag{42}$$

5.3. Complexity Analysis

As complex multiplication (CM) stands as one of the most computationally intensive arithmetic operations in practice, we assess the arithmetic load of the proposed NSSS synchronization method in terms of the number of CMs. To ensure a fair comparison with conventional detection methods, we assume that the complexity of single CM is equal to that of six real multiplications (RMs) [25]. Let N_a be the number of average estimates.

First, we evaluate the arithmetic complexity of the RPCD approach. Due to the conjugate symmetric property of the ZC sequence with respect to the origin, (35) necessitates $N_s/2$ CMs, with 252 hypotheses requiring CM operations. When applying average estimation N_a times, the RPCD method identifies the PCID using $16632N_a$ CMs. As previously mentioned, the DPCD method utilizes both the observations (38) and (35), but with $Y_l(m)$ replaced by $\hat{Y}_l(m)$. For each trial, (38) needs N_s CMs to compute the correlation $\sum_{l=3}^{13}Y_l(m)C_l^{\tilde{n},\tilde{u},\tilde{w}*}(m)$ and $N_s/11$ CMs to implement the argument operation $\angle\{\cdot\}$. On the other hand, $2N_s/11$ RMs are utilized for $\Re\{\sum_{l=3}^{13}\sum_{m\in\mathcal{S}}\hat{Y}_l(m)C_l^{\tilde{n},\tilde{u},\tilde{w}*}(m)\}$ since some quantities have been previously evaluated in (38). Considering all hypotheses, the total complexity of the DPCD method becomes $97776N_a$ CMs. In the case of the SPCD method, we need $252N_s$ CMs to estimate the channel for 252 hypothesized values and $4032N_s/11$ RMs to compute (41) for 2016 hypothesized values in the first stage. As multiplication operations are not required in the second step, the total count of CMs is given by $41328N_a$ in the case of the SPCD method.

Finally, we evaluate the arithmetic complexity of the proposed approach. For every trial, the computation of the quantity $\bar{Y}_l^{\tilde{n},\tilde{u},\tilde{w}}(m)$ involves N_s CMs, and the blockwise correlation (6) requires only 12 CMs. Similar to the RPCD, as (6) needs to be hypothesized for 252 combinations, the proposed method necessitates $36864N_a$ CMs. It is interesting to note that the conventional RCFO estimation method requires $12(11 - D_t)$ CMs, while the proposed RCFO estimation method eliminates the need for CMs, utilizing the same cost function used for PCID detection.

5.4. Performance Analysis

In Figure 2, the detection probability $\text{Prob}\{(\hat{n}, \hat{u}, \hat{w}) = (n, u, w)\}$ is presented for both the DPCD and proposed synchronization methods versus average SNR, considering both AWGN and flat-fading conditions. The scenarios when $\varepsilon = \eta = 0$ and the channel is ideally estimated are examined. Although not depicted in Figure 2, the detection curves of both the DPCD and SPCD schemes exhibit remarkable similarity, which can be attributed to the fact that both approaches are derived from a similar coherent cost function. It is worth emphasizing that the proposed NSSS synchronization method equipped with the optimal value of $N_b = 5$ appears to achieve superior detection performance to the conventional method. Analytical curves of the proposed and DPCD methods are plotted according to (25) and (39), respectively. As expected, averaging multiple NSSS observations can be adopted to mitigate the influence of noise on the final estimate. These observations provide sufficient evidence to support the usefulness of the proposed NSSS synchronization method and the accuracy of the theoretical expression derived in Section 4.2.

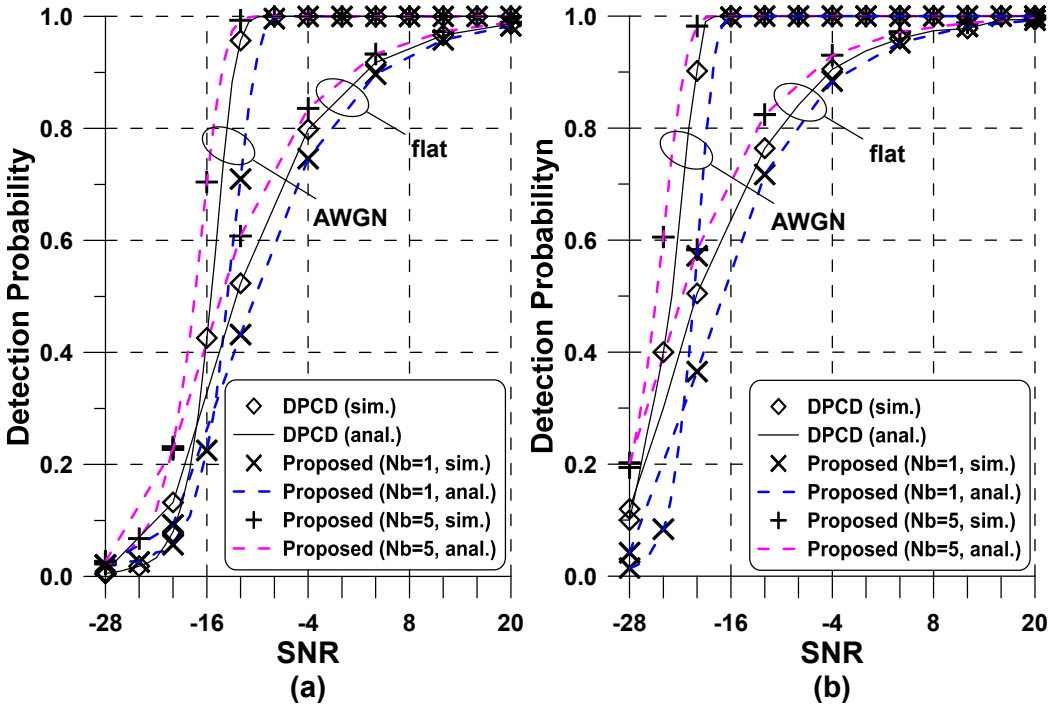

Figure 2. Performance of the proposed NSSS detection schemes in AWGN and flat-fading channels: (**a**) $N_a = 1$; (**b**) $N_a = 10$.

In Figure 3, we present the detection probability of both the benchmark and proposed NSSS detection schemes. We consider the proposed method equipped with $N_b = 5$. To compare the performance between these approaches, we define the number of radio frames needed to attain a target detection probability of 90% as N_t. For the vehicular channel scenario under a poor coverage condition of SNR $= -5$ dB, the number of radio frames involved to obtain a detection probability of 90% becomes $N_t = 7$ for the RPCD, $N_t = 4$ for the SPCD, and $N_t = 5$ for the proposed approach. When compared with

the proposed approach, the SPCD method shows similar complexity and performance, while the RPCD method requires a significantly longer processing time. In the pedestrian channel, the noncoherent RPCD method exhibits superior performance compared with other coherent detection methods, while the proposed method outperforms both the SPCD and DPCD methods. As the frequency selectivity of the fading channel increases, the noncoherent RPCD method exhibits lower detection capability. When considering the same value of N_t, the proposed method requires 10.8% fewer CMs than the SPCD method, but it requires 2.2 times more CMs than the RPCD method. These observations demonstrate that the proposed method effectively strikes a better trade-off between detection performance and computational complexity for various channel fading conditions. One distinctive advantage of the proposed method, unlike other approaches, is the potential to implement the RCFO estimator using the same cost function employed for PCID detection, which will be explained subsequently.

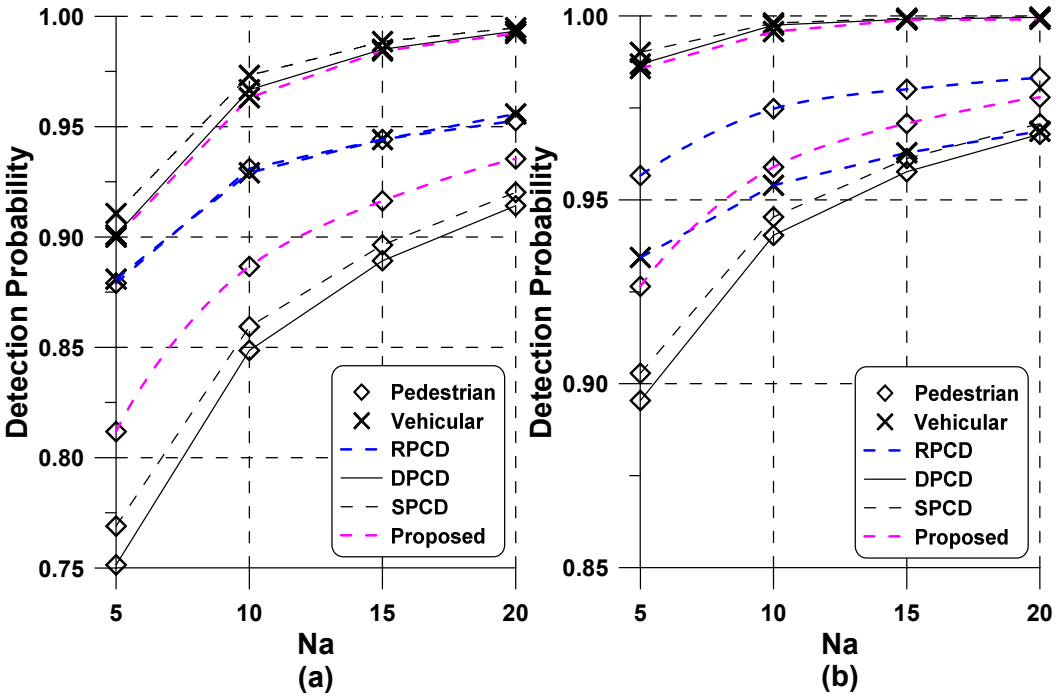

Figure 3. Performance comparison between the conventional and proposed NSSS detectors as a function of N_a: (**a**) SNR $= -5$ dB; (**b**) SNR $= 0$ dB.

Figure 4 provides a comparison of the MSE performance of the RCFO estimators in the pedestrian channel. For a fair comparison, in the case of the conventional RCFO method, D_t is set to 5 or 6 in (41) to have the same estimation range as the proposed RCFO method. The analytical MSE of the proposed and conventional estimators is based on (34) and (42), respectively. It can be evident from Figure 4a that the MSE of the proposed approach is heavily influenced by the design parameter N_b, but it shows superior performance compared with the benchmark scheme. As expected, both RCFO estimation methods exhibit an irreducible MSE caused by the presence of RCFO as the SNR value increases. More interestingly, it can be observed from Figure 4b that the MSE of the proposed RCFO synchronization scheme is optimal when the block size N_b is 5 or 6, and these integer values coincide with the optimal integer values obtained in Section 4.2. Moreover, the analytical MSE demonstrates a good match with the simulated MSE even in the presence of a frequency offset value of $\varepsilon = 0.1$.

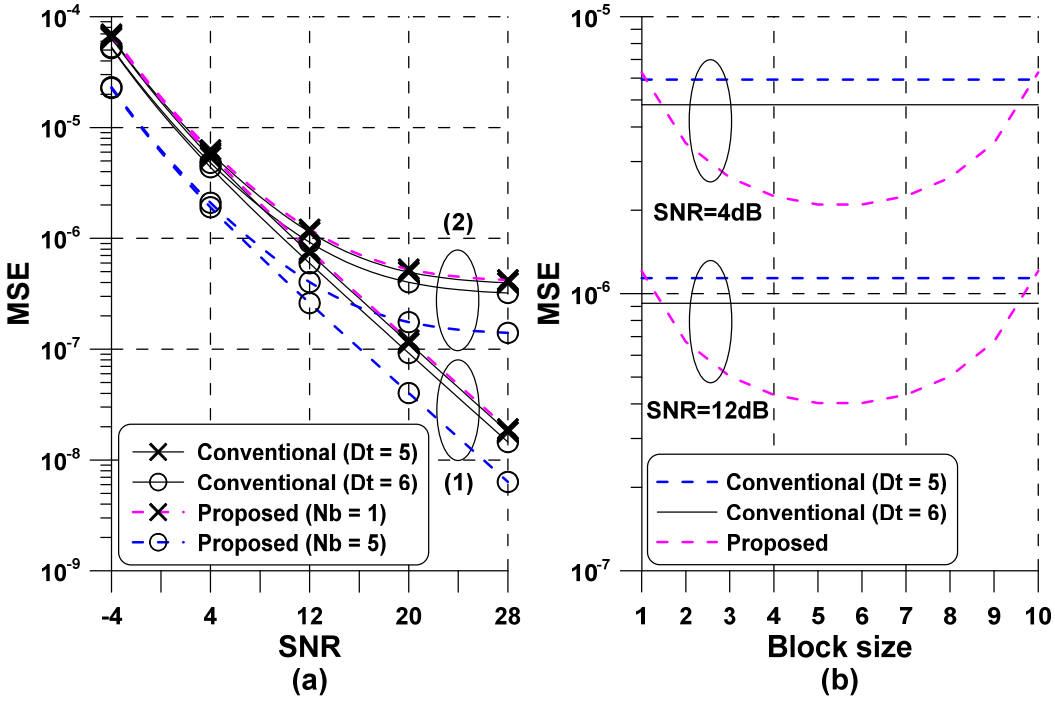

Figure 4. Performance of the RCFO synchronization schemes in the pedestrian channel: (**a**) versus SNR (1) $\varepsilon = 0.0$ (2) $\varepsilon = 0.1$; (**b**) versus N_b .

6. Concluding Remarks

This paper proposes a synchronization scheme for joint PCID and RCFO using the NSSS in the cellular NB-IoT system. The investigated method offers the advantage of simultaneously estimating RCFO by utilizing the same cost function employed for PCID detection. Numerical results were presented to confirm not only the accuracy of the derived detection probability and MSE of the proposed method but also its superior performance. It has been verified that the derived theoretical performance and simulation results are identical. Furthermore, we conducted a performance comparison between the proposed and conventional NSSS detectors, focusing on factors such as arithmetic complexity and detection capability. The benefits of the proposed PCID and RCFO synchronization scheme have been validated via simulation experiments, confirming its superior performance while maintaining relatively lower complexity compared with conventional NSSS synchronization schemes. To achieve a detection probability of 90% in the frequency-selective fading channel, it has been experimentally demonstrated that the proposed method reduces the number of CMs by over 30% under poor coverage conditions compared with the DPCD method.

Finally, future work comprises new strategies to address the robustness and complexity concerns associated with the presented synchronization receiver. Given the limitations of a noncoherent detection approach in effectively mitigating frequency-selective fading distortion, enhancements are necessary to ensure improved performance. Of particular significance is the development of an ultraextended coverage solution tailored for extremely poor channel conditions. Under these circumstances, existing detection methods exhibit inefficiency with respect to processing delay, resulting in elevated power consumption.

Author Contributions: Conceptualization, Y.-H.Y. and Y.-A.J.; methodology, Y.-H.Y. and Y.-A.J.; software, Y.-A.J.; writing—original draft preparation, Y.-H.Y. and Y.-A.J.; writing—review and editing, Y.-H.Y., Y.-A.J., S.-H.L. and I.H.; visualization, Y.-H.Y. and Y.-A.J.; supervision, Y.-H.Y. All authors have read and agreed to the published version of the manuscript.

Funding: This work was in part supported by the National Research Foundation of Korea (NRF) grant funded by the Korean government (MSIT) (No. RS-2023-00219051) and in part supported by the Institute of Information and Communications Technology Planning and Evaluation (IITP) grant funded by the Korean government (MSIT) (2022-0-00162, Development of Industrial 5G Private Network Management System).

Institutional Review Board Statement: Not applicable.

Informed Consent Statement: Not applicable.

Data Availability Statement: Not applicable.

Conflicts of Interest: The authors declare no conflict of interest.

References

1. 3GPP, TR 36.888. Study on Provision of Low-Cost Machine-Type Communications (MTC) User Equipments (UEs) Based on LTE; Sophia Antipolis, France, 2013. Available online: https://portal.3gpp.org/desktopmodules/Specifications/SpecificationDetails.aspx?specificationId=2578 (accessed on 25 July 2023).
2. Haider, S.K.; Nauman, A.; Jamshed, M.A.; Jiang, A.; Batool, S.; Kim, S.W. Internet of drones: Routing algorithms, techniques and challenges. *Mathematics* **2022**, *10*, 1488. [CrossRef]
3. Chen, X.; Zhao, T.; Sun, Q.; Hu, Q.; Xu, M. Cell-free massive MIMO with energy-efficient downlink operation in industrial IoT. *Mathematics* **2022**, *10*, 1687. [CrossRef]
4. Almuhaya, M.A.M.; Jabbar, W.A.; Sulaiman, N.; Abdulmalek, S. A Survey on LoRaWAN technology: Recent trends, opportunities, simulation tools and future directions. *Electronics* **2022**, *11*, 164. [CrossRef]
5. 3GPP, 3GPP TS 36.211. Physical Channels and Modulation (Release 14). Tech. Rep.; Sophia Antipolis, France, 2017. Available online: https://www.etsi.org/deliver/etsi_ts/136200_136299/136211/14.02.00_60/ts_136211v140200p.pdf (accessed on 25 July 2023).
6. Lee, B.M. Enhancing IoT connectivity in massive MIMO networks through systematic scheduling and power control strategies. *Mathematics* **2023**, *11*, 3012. [CrossRef]
7. Ikpehai, A.; Adebisi, B.; Rabie, K.M.; Anoh, K.; Ande, R.E.; Hammoudeh, M.; Gacanin, H.; Mbanaso, U.M. Low-power wide area network technologies for Internet-of-Things: A comparative review. *IEEE Internet Things J.* **2019**, *6*, 2225–2240. [CrossRef]
8. Keshta, I.; Soni, M.; Bhatt, M.; Irshad, A.; Rizwan, A.; Khan, S.; Maaliw, R., III; Soomar, A.M.; Shabaz, M. Energy efficient indoor localisation for narrowband internet of things. CAAI Trans. *Intell. Technol.* **2023**, 1–14. [CrossRef]
9. Chang, K.; Lee, S. Robust OFDM-based synchronization against very high fractional CFO and time-varying fading. *IEEE Syst. J.* **2020**, *14*, 4047–4058. [CrossRef]
10. Kroll, H.; Korb, M.; Weber, B. Maximum-Likelihood detection for energy-efficient timing acquisition in NB-IoT. In Proceedings of the IEEE Wireless Communications and Networking Conference Workshops (WCNCW 2017), San Francisco, CA, USA, 19–22 March 2017.
11. Yang, W.; Hua, M.; Zhang, J.; Xia, T.; Zou, J.; Jiang, C.; Wang, M. Enhanced system acquisition for NB-IoT. *IEEE Access* **2017**, *5*, 13179–13191. [CrossRef]
12. Intel Corporation. *Synchronization and Cell Search in NB-IoT: Performance Evaluation*; 3GPP TSG RAN WG1, Tech. Rep. Tech. Rep. R1-161898; Intel Corporation: Santa Clara, CA, USA, 2016.
13. Wang, Y.P.E.; Lin, X.; Adhikary, A.; Grovlen, A.; Sui, Y.; Blankenship, Y.; Bergman, J.; Razaghi, H.S. A primer on 3GPP narrowband Internet of Things. *IEEE Commun. Mag.* **2017**, *55*, 117–123. [CrossRef]
14. Ali, A.; Hamouda, W. On the cell search and initial synchronization for NB-IoT LTE systems. *IEEE Commun. Lett.* **2017**, *21*, 1843–1846. [CrossRef]
15. Li, Y.; Chen, S.; Ye, W.; Lin, F. A joint low-power cell search and frequency tracking scheme in NB-IoT systems for green Internet of Things. *Sensors* **2018**, *18*, 3274. [CrossRef] [PubMed]
16. Savaux, V. DFT-based low-complexity optimal cell ID estimation in NB-IoT. *EURASIP J. Adv. Signal Process.* **2020**, *2020*, 14. [CrossRef]
17. Savaux, V.; Kanj, M. Low-complexity sub-optimal cell ID estimation in NB-IoT system. *IET Commun.* **2020**, *14*, 3699–3706. [CrossRef]
18. You, Y.H.; Jung, Y.A.; Lee, S.H.; Hwang, I. Complexity-efficient coherent physical cell identity detection method for cellular IoT systems. *Mathematics* **2022**, *10*, 3024. [CrossRef]
19. Rotem, A.; Dabora, R. A novel low-complexity estimation of sampling and carrier frequency offsets in OFDM communications. *IEEE Access* **2020**, *8*, 194978–194991. [CrossRef]
20. Popovic, B.M. Generalized chirp-like polyphase sequences with optimum correlation properties. *IEEE Trans. Inf. Theory* **1992**, *30*, 769–777. [CrossRef]
21. Wang, X.; Hu, B. A low-complexity ML estimator for carrier and sampling frequency offsets in OFDM systems. *IEEE Commun. Lett.* **2014**, *18*, 503–506. [CrossRef]

22. International Telecommunication Union. *Guidelines for Evaluation of radio Transmission Technologies for IMT-2000. ITU-R M. 1225-97*; International Telecommunication Union: Geneva, Switzerland, 1997.
23. Jewel, M.K.H.; Zakariyya, R.S.; Lin, F. On channel estimation in LTE-based downlink narrowband Internet of Things systems. *Electronics* **2021**, *10*, 1246. [CrossRef]
24. Holfeld, B.; Wieruch, D.; Wirth, T.; Thiele, L.; Ashraf, S. A.; Huschke, J.; Aktas, I.; Ansari, J. Wireless communication for factory automation: An opportunity for LTE and 5G systems. *IEEE Commun. Mag.* **2016**, *54*, 36–43. [CrossRef]
25. Golub, G.H.; Loan, C.F.V. *Matrix Computations*, 4th ed.; The Johns Hopkins University Press: Baltimore, MD, USA, 2013.